6-1-2009

On the Mechanisms of Episodic Salinity Outflow Events in the Strait of Hormuz

Prasad G. Thoppil
University of Southern Mississippi, thoppil@nrlssc.navy.mil

Patrick J. Hogan
Stennis Space Center

On the Mechanisms of Episodic Salinity Outflow Events in the Strait of Hormuz

Prasad G. Thoppil*

Department of Marine Science, University of Southern Mississippi, Stennis Space Center, Mississippi

Patrick J. Hogan

Ocean Monitoring and Prediction System Section, Naval Research Laboratory, Stennis Space Center, Mississippi

ABSTRACT

Observations in the Strait of Hormuz (26.26°N, 56.08°E) during 1997–98 showed substantial velocity fluctuations, accompanied by episodic changes in the salinity outflow events with amplitude varying between 1 and 2 psu on time scales of several days to a few weeks. These events are characterized by a rapid increase in salinity followed by an abrupt decline. The mechanisms behind these strong pulses of salinity events are investigated with a high-resolution (~1 km) Hybrid Coordinate Ocean Model (HYCOM) with particular reference to the year 2005. In accordance with the observations, the simulated salinity events are characterized by strong coherence between the enhanced flows in zonal and meridional directions. It is inferred that most of the simulated and observed outflow variability is associated with the continuous formation of strong mesoscale cyclonic eddies, whose origin can be traced upstream to around 26°N, 55.5°E. These cyclonic eddies have a diameter of about 63 km and have a remnant of Persian Gulf water (PGW) in their cores, which is eroded by lateral mixing as the eddies propagate downstream at a translation speed of 4.1 cm s^{-1}. The primary process that acts to generate mesoscale cyclones results from the barotropic instability of the exchange circulation through the Strait of Hormuz induced by fluctuations in the wind stress forcing. The lack of salinity events and cyclogenesis in a model experiment with no wind stress forcing further confirms the essential ingredients required for the development of strong cyclones and the associated outflow variability.

1. Introduction

The Persian Gulf (also known as the Arabian Gulf) is a semienclosed shallow sea (average depth is about 35 m) characterized by significant evaporation [1–2 m yr^{-1}, Privett (1959); Meshal and Hassan (1986)] and is connected to the Gulf of Oman and the Arabian Sea through the Strait of Hormuz (Fig. 1). High evaporation and strong surface heat loss in the gulf during winter (November–February) combined with restricted exchange with the open ocean lead to the convective formation of the saltier and denser Persian Gulf water (PGW) mass. The densest water forms during winter in the northern end of the gulf, where it has a salinity of about 41 psu and temperature maxima higher than 21°C (Swift and Bower 2003). The resulting water deficit in the gulf is compensated for by an inflow of relatively warmer and less saline water of Arabian Sea origin (36.5–37 psu) through the Strait of Hormuz. The low-salinity inflow occurs along the northern side of the strait and spreads westward along the Iranian coast (Brewer et al. 1978; Hunter 1986; Reynolds 1993). The high-salinity outflow through the Strait of Hormuz is mostly confined to the southern part of the strait (Chao et al. 1992; Johns et al. 2003). Unlike other semienclosed basins, the Persian Gulf is shallow (<100 m) and there is no prominent sill to constrain the outflow. However, farther upstream from the strait, a sill in the vicinity of 26°N, 55.4°E (80-m isobaths) appears to constrain the circulation and water mass exchange process (Fig. 1) and does have an impact on the outflow variability, which we discuss in this paper.

The winds over the Persian Gulf are northwesterly or westerly throughout the year and are strongest during winter (Fig. 2). Swift and Bower (2003) suggested that

* Current affiliation: Planning Systems Incorporated, Stennis Space Center, Mississippi.

Corresponding author address: Prasad Thoppil, Naval Research Laboratory, Code 7323, Stennis Space Center, MS 39529.
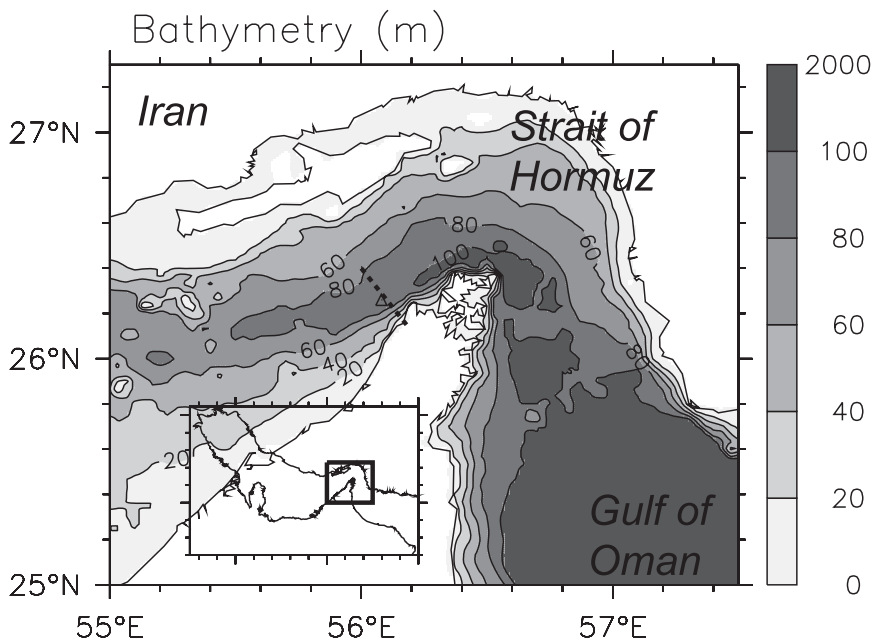E-mail: thoppil@nrlssc.navy.mil

FIG. 1. Model bathymetry of the Strait of Hormuz in meters. Johns et al. (2003) observation location of the ADCP and temperature–salinity profile moorings is indicated by the triangle (26.26°N, 56.08°E) and four hydrographic sections in the southern part of the strait are marked with a dotted line. The region inset shows the Persian Gulf model domain. Bathymetry is contoured in 20-m intervals to 100 m.

the sea surface height difference between the Persian Gulf and the Gulf of Oman controls the inflow–outflow transport through the Strait of Hormuz, but other studies have indicated baroclinic forcing due to the density difference as the driving force (Chao et al. 1992). Net evaporation over the Persian Gulf shows a seasonal cycle (Chao et al. 1992) and that cycle could lead to a seasonal variation of the water exchange through the strait. However, there is no agreement from models or observations on whether such a seasonal cycle exists

(Chao et al. 1992; Reynolds 1993; Horton et al. 1994; Banse 1997; Bower et al. 2000; Swift and Bower 2003; Johns et al. 2003).

Johns et al. (2003) investigated the exchange between the Persian Gulf and the Gulf of Oman using hydrographic and moored acoustic Doppler current profiler (ADCP) data from the Strait of Hormuz (26.26°N, 56.08°E) during the period of December 1996–March 1998. Despite discontinuities in the current meter records, their moored time series showed a relatively
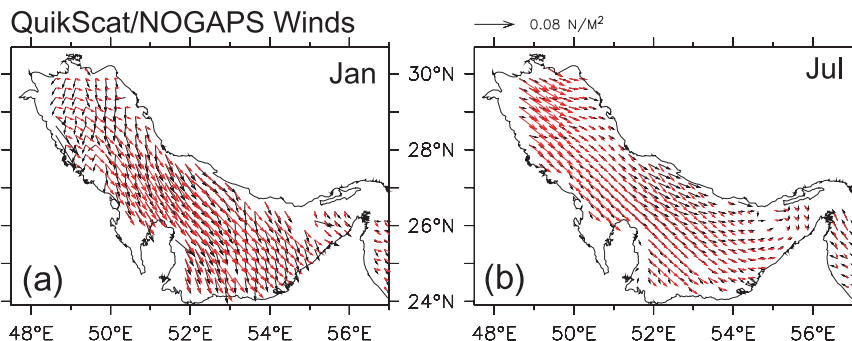

FIG. 2. A comparison of wind stress derived from the QuikSCAT (black vectors) and ½° NOGAPS (red vectors) for (a) January 2005 and (b) July 2005 in N m^{-2}. The 3-hourly, ½° NOGAPS wind stress is interpolated to a daily ¼° QuikSCAT grid. A constant drag coefficient (C_D) value of 1.2×10^{-3} is used to compute the wind stress from the QuikSCAT wind velocity. A daily QuikSCAT wind stress has been generated by taking 3-day moving averages.
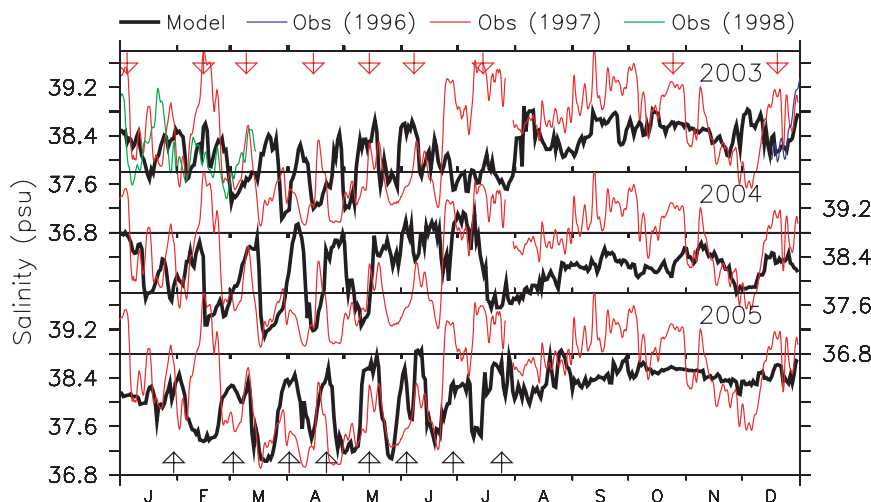
FIG. 3. Episodic events of high-salinity outflow at 26.26°N, 56.08°E inferred from the model during 2003–05 and from observations by Johns et al. (2003) during December 1996–March 1998. Salinities at 40 m for 2003–05 are shown as a thick line. Observed salinities at the same depth during 1996 (blue line), 1997 (red line), and 1998 (green line) are included. Observed salinity, which is sampled at 30 s, is applied with a 2-day Parzen smoothing to highlight the episodic variations in the high-salinity outflow. Red and black arrows mark periods of increased salinity outflow events seen in the observations during 1997 and in the model during 2005. Observed salinity during 1997 is repeated with the model salinity during 2003–05.

steady deep outflow through the strait from 40 m to the bottom with a mean speed of approximately 20 cm s^{-1}. A variable flow was found in the upper layer with frequent reversals on time scales of several days to weeks. The estimated annual mean bottom outflow transport through the strait was 0.15 ± 0.03 Sv (1 Sv ≡ 10^6 m^3 s^{-1}). More recently, Pous et al. (2004a,b) studied the hydrology and circulation in the Strait of Hormuz and the Gulf of Oman using observations for the period of October–November 1999. They also observed outflow variability at the Strait of Hormuz over a 2–3-week period.

Johns et al.'s (2003) observation is the only well-sampled time series data in the Strait of Hormuz that can be used to resolve the highly variable salinity outflow at periods of several days to weeks. Figure 3 shows the observed salinity at 40 m at 26.26°N, 56.08°E during December 1996–March 1998 (Johns et al. 2003). There were several pulselike events of high salinity (hereafter denoted as the salinity events) evident throughout the period, but predominantly between February and July. Note that salinity events are more pronounced at this depth than at the surface. These events were characterized by a rapid increase in salinity followed by a sudden decrease and had a time period of 15–30 days on average. The amplitudes of these episodic salinity events often reached ~1.5–2.5 psu.

The goal of this paper is to understand the remarkable episodic events of high-salinity outflow that have been observed in the Strait of Hormuz by Johns et al.

(2003) and to examine the physical processes leading to such variability. The main tool that we use here is a regional, high-resolution Hybrid Coordinate Ocean Model (HYCOM). The rest of the paper is organized as follows. The model configuration and surface forcing are discussed in section 2. An examination of the circulation and hydrography in the Strait of Hormuz offers some clues as to the processes that govern the exchange through the strait, which is discussed in section 3a. The evidence for the observed and simulated variabilities in the outflow is presented in section 3b and the underlying physical processes in generating such variabilities are discussed in section 3c. The transport estimate across the strait is presented in section 3d. The results are briefly summarized in section 4.

2. Model description

The model used is HYCOM (Bleck et al. 2002), with a horizontal resolution of ~1 km (0.01°) and which is thus capable of resolving mesoscale eddies realistically. There are 16 hybrid layers in the vertical with density values (sigma units): 19.5, 20.25, 21, 21.75, 22.5, 23.25, 24, 24.7, 25.28, 25.77, 26.18, 26.6, 26.95, 27.3, 27.65, and 28. The top layer minimum thickness is 3 m. The model domain extends northward from 22.7°N and westward from 59.4°E and has 1217 × 945 × 16 grid points. The baroclinic (barotropic) time step is 60 s (3 s). The bathymetry used in the model is derived from the Digital

Bathymetry Data Base 2-min resolution topography (DBDB2). Minimum water depth is chosen at 2 m, but the 0-m contour describes the land–sea boundary. A Mercator grid projection is used. The eastern boundary is treated as closed, but is outfitted with a 50-grid-point buffer zone (~0.5°) in which temperature, salinity, and pressure are relaxed toward the General Digital Environmental Model (GDEM3) seasonally varying climatology with an *e*-folding time scale of 1–76 days. The monthly river inflow into the basin is prescribed as precipitation (Shatt-al-Arab, Karun, Karkkeh, Jarrahi, Zohreh and Minab). A major source of river discharge into the basin occurs at the head of the gulf, known as the Shatt-al-Arab.

The model integration was started from rest on 1 January 2000 and initialized with temperature and salinity from the GDEM3 climatology. The model is driven by fields of 10-m wind speed, vector wind stress, 2-m air temperature, 2-m atmospheric humidity, surface shortwave and longwave heat fluxes, and precipitation. These fields are extracted from the 3-hourly 1° horizontal resolution Navy Operational Global Atmospheric Prediction System (NOGAPS) reanalysis product. The use of high-frequency (3 h) atmospheric forcing (except solar radiation, which is daily) to correctly reproduce the observed circulation and outflow are found to be important. Surface latent and sensible heat fluxes, along with evaporation, are calculated by employing bulk formulas during the model run time using model SST (Kara et al. 2002). This has an implied restoring term, pulling the model-produced SST toward the specified air temperature, thereby minimizing the model SST drift. It should be noted that in all simulations sea surface salinity is restored to the GDEM3 monthly climatology with a time scale of ~30 days. As a result, the simulated salinity events only qualitatively agree with the observations. The simulations included the National Aeronautics and Space Administration (NASA) Goddard Institute for Space Studies (GISS) level 2 vertical mixing scheme, which was constructed using the Reynolds stress model (Canuto et al. 2001, 2002, 2004).

The model is run for 6 yr covering the period of 2000–05 using 1° NOGAPS atmospheric forcing. The model run is then repeated with 3-hourly, ½° NOGAPS forcings for the period 2003–05. The ½° NOGAPS forcing fields are corrected for land contamination near the land–sea boundaries (Kara et al. 2007). An additional correction is applied to the magnitude of the wind using Quick Scatterometer (QuikSCAT) winds. These corrections lead to improvements in the overall circulation especially near the coast. A comparison of NOGAPS wind stress with that derived from QuikSCAT during January and July 2005 (Fig. 2) suggests that model forcings are adequate. The magnitude of the wind stress is strong in January and weak in July both in the QuikSCAT and NOGAPS data, although differences exist in some regions. The differences between QuikSCAT and NOGAPS may result partly from the frequency of the wind observations; 3-hourly NOGAPS versus 3-day running mean QuikSCAT winds. The estimated annual mean air–sea heat flux is very much in agreement with Johns et al.'s (2003) estimate. The basin-averaged (west of 56°E) annual mean net heat flux from the model is -3 W m^{-2}; that is, a net heat loss of 3 W m^{-2} from the ocean for the period 2003–05. This value is closer to the basin-averaged loss of -7 ± 4 W m^{-2} obtained from the estimates of advective heat fluxes through the strait by Johns et al. (2003). The basin-averaged climatological annual mean heat flux from the Southampton Oceanography Centre (SOC) air–sea flux climatology is an ocean gain of 60 W m^{-2}. However, Johns et al.'s (2003) careful evaluations of the SOC fields resulted in a smaller annual mean ocean heat gain of 4 W m^{-2}, which is closer to that derived from the advective budget. The various corrections applied to the SOC fields are described at length by Johns et al. (2003).

3. Results

Since our goal is to simulate the episodic variations in the salinity outflow similar to those observed in the strait, model results from a particular year would be an ideal choice. Since our simulation period did not include the period of observations (1997–98) that were made, an attempt has been made 1) to make sure that the characteristics of the simulated salinity events are similar to the observations and 2) to point out that the interannual variability of the salinity episodes is large. Figure 3 shows the simulated salinity at 40 m at 26.26°N, 56.08°E during 2003–05 and the observed salinity for December 1996–March 1998. The model-simulated salinity events are consistent with the observations; each event is characterized by a rapid increase in salinity followed by a sharp decline. However, the amplitude, the time of occurrence, and the number of salinity events vary significantly from year to year. A comparison of salinity events during January–March 1997 and 1998 also gives an indication to the possible interannual variability; observations in mid-February 1997 indicated a strong event with salinity exceeding 39.2 psu, but this event was not observed in 1998. This seems to be an indication of salinity events being influenced by atmospheric forcing.

The similarities of the salinity events simulated by the model and the observations give us confidence in the model's ability to reproduce them. Furthermore, the time

of occurrence of some of the model-simulated events during 2005 coincides with those in the observations. In particular, the salinity events, which are evident in both the observations and the model during early March and late July, can be delineated by comparing the model fields to the hydrographic and ADCP sections across the southern part of the strait (Johns et al. 2003). Therefore, it makes sense to consider the results from the last year (2005) of the model run. The model outputs were saved daily, from which a monthly mean climatology was prepared. The basin-averaged temperature for the period 2000–05 indicated that the model had reached a steady state by 2005. Furthermore, the Persian Gulf is a relatively shallow basin, having an average depth of 35 m with a maximum depth of ~100 m (except in the Gulf of Oman). Therefore, the model fields analyzed from the year 2005 are not influenced by the initial conditions.

A time series of basin-averaged (region west of 57°E) sea surface temperature (SST), salinity (SSS), and mean kinetic energy (MKE, $\times 10^{-2}$ m^2 s^{-2}) during the period of 2003–05 is shown in Fig. 4. Also included in Fig. 4a is the SST derived from the 4-km Moderate Resolution Imaging Spectrometer (MODIS) observations for the same period. Superimposed on Fig. 4b is the annual cycle of SSS from the GDEM3 climatology. The agreements between the observed and model SST are fairly good, with the model SST being somewhat colder during winter. The annual cycle of SST closely follows the annual cycle of solar radiation, with a minimum during winter (~17°C) and a maximum during summer (~32°C). Like SST, SSS clearly shows an annual cycle. The formation of the hypersaline PGW peaks in February–March, consistent with the evaporation and net surface heat loss from the ocean. Due to intense mixing of PGW with the inflowing fresher water from the Gulf of Oman, the SSS decreases steadily from April through August. The salinity minimum in the GDEM3 climatology occurs in July, which is 1 month earlier than that in the model. The reason for such a model–data discrepancy is unclear, but will be investigated in the future. The MKE shows a seasonal pattern very similar to that for SST with its highest level of energy of the mean flow during the summer (June, ~2.5×10^{-2} m^2 s^{-2}) and lowest during winter (January, ~0.8×10^{-2} m^2 s^{-2}). The low MKE during winter, despite a moderate increase in the wind speed, is possibly associated with the vertically homogeneous and weakly stratified water column. The development of the thermocline and strong stratification during summer increase the mean energy through geostrophy and Ekman flow. A higher level of kinetic energy is evident during 2003 and 2005 in comparison with 2004.
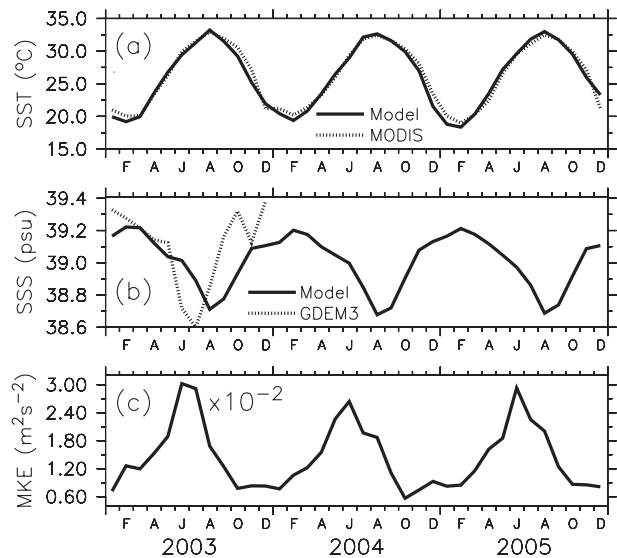

FIG. 4. Time series of basin-averaged (west of 57°E) monthly mean (a) SST (°C), (b) SSS (psu), and (c) MKE ($\times 10^{-2}$ m^2 s^{-2}) from the last three years (2003–05) of the model run. For comparison, SSTs derived from the 4-km MODIS for the same period (2003–05, dotted line) and SSS from the GDEM3 climatology are included (dotted line).

a. Circulation and exchange in the Strait of Hormuz

The circulation in the upper 40 m through the Strait of Hormuz is presented in Fig. 5. The flows within the strait are highly variable in both magnitude and direction. The flow is relatively weak during winter. Overall, a cyclonic recirculation cell is the predominant feature of the circulation. A significant part of the surface outflow that leaves the strait at the southern part of the channel joins the inflow from the Gulf of Oman. The eastern extent of this returning flow shows high temporal variability, changing from 56.8°E in April to 56.2°E in September. The spatial extent of the inflow from the Gulf of Oman also shows high variability. On several occasions, part of the surface flow that enters the strait in the north bifurcates at 56°E with a branch joining with the outflow and another branch continuing into the Persian Gulf (April–May, August). The circulation during August–October shows an anticyclonic eddy situated northeast of the surface inflow. This complex circulation could have important consequences for the exchange process and for mesoscale variability.

Although most of these simulated circulation features cannot be verified against observations, we compare sections of the model-derived temperature, salinity, and velocity fields with those observed across the southern part of the strait by Johns et al. (2003). Figure 6 shows the observed salinity and along-strait velocity during 16 March 1998, 11 March 1997, 28 July 1997, and
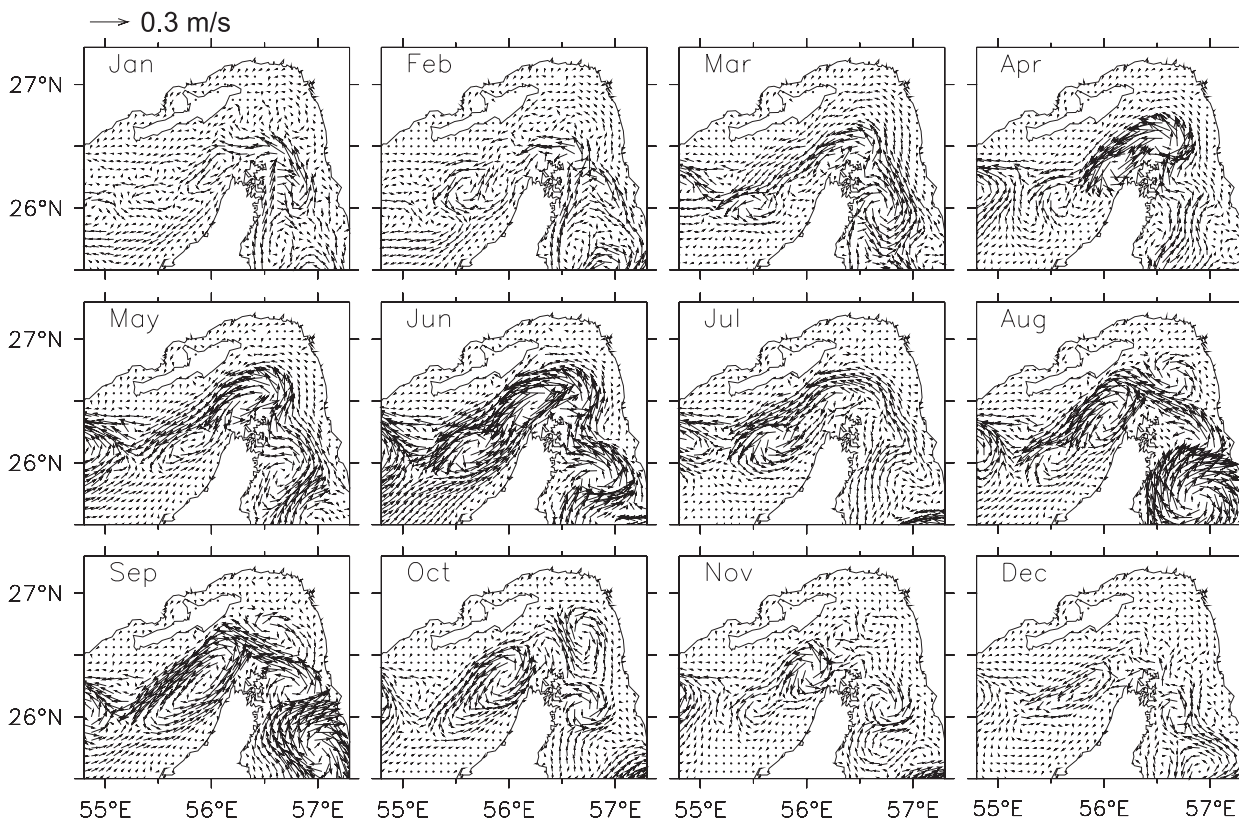
FIG. 5. Monthly mean currents in the upper 40 m (averaged for the upper 40 m) for the Strait of Hormuz from the last year (2005) of the model run.

15 December 1997, as shown by Johns et al. (2003) in their Figs. 10a and 10b. It should be noted that the velocity sections were detided using the method detailed by Johns et al. (2003) due to the strong tidal currents in the strait. Model salinity and velocity cross sections across the strait during 10 March, 14 March, 27 July, and 15 December 2005 are displayed in Fig. 7. Also shown in Figs. 7i–l are currents in the upper 40 m superimposed on the salinity at 20 m from the model for the same period. The times of these sections are chosen to match the times of the observations and the features that we want to emphasize. This comparison should be regarded as qualitative because the observations were made in 1997–98 and the model is forced with 2005 atmospheric conditions. It should be noted that the Johns et al. (2003) sections extended only ~32 km across the southern part of the Strait of Hormuz.

The characteristics of salinity and flow pattern across the strait simulated by the model generally agree with the observations with two exceptions. First, the salinity maximum in the model is underestimated by 1–1.5 psu due to the relaxation of the surface salinity to the GDEM3 climatology. Second, the model outflow velocity is relatively weaker than the observations by

15–25 cm s^{-1}. This may be because the observed along-strait velocity sections were detided using the tidal current information contained in the moored ADCP records according to the procedure described by Johns et al. (2003).

Besides strong interannual variability in the observed outflow currents, the peak outflow with its core located below 40 m occurred along the southern part of the strait during March. The along-strait velocity ranged from 30 cm s^{-1} during 16 March 1998 to 50 cm s^{-1} on 11 March 1997. During this period, there was a surface inflow in the upper 60 m north of ~26.3°N, though the velocity was marginally stronger (-30 cm s^{-1}) during 16 March 1998. The spatial characteristics of the outflow (25 cm s^{-1}) and the inflow (-20 cm s^{-1}) from the model are analogous to those in the observations. Both the observed and simulated salinity contours are concentrated on the southern side of the strait, which entirely reflects the density stratification. This sloping isopycnal gives rise to an across-channel pressure gradient, which is balanced by the along-channel geostrophic velocity.

An intriguing feature of the current in the near-surface layer is that it shows large-amplitude short-term variations with occasional reversals. For instance, Johns et al.
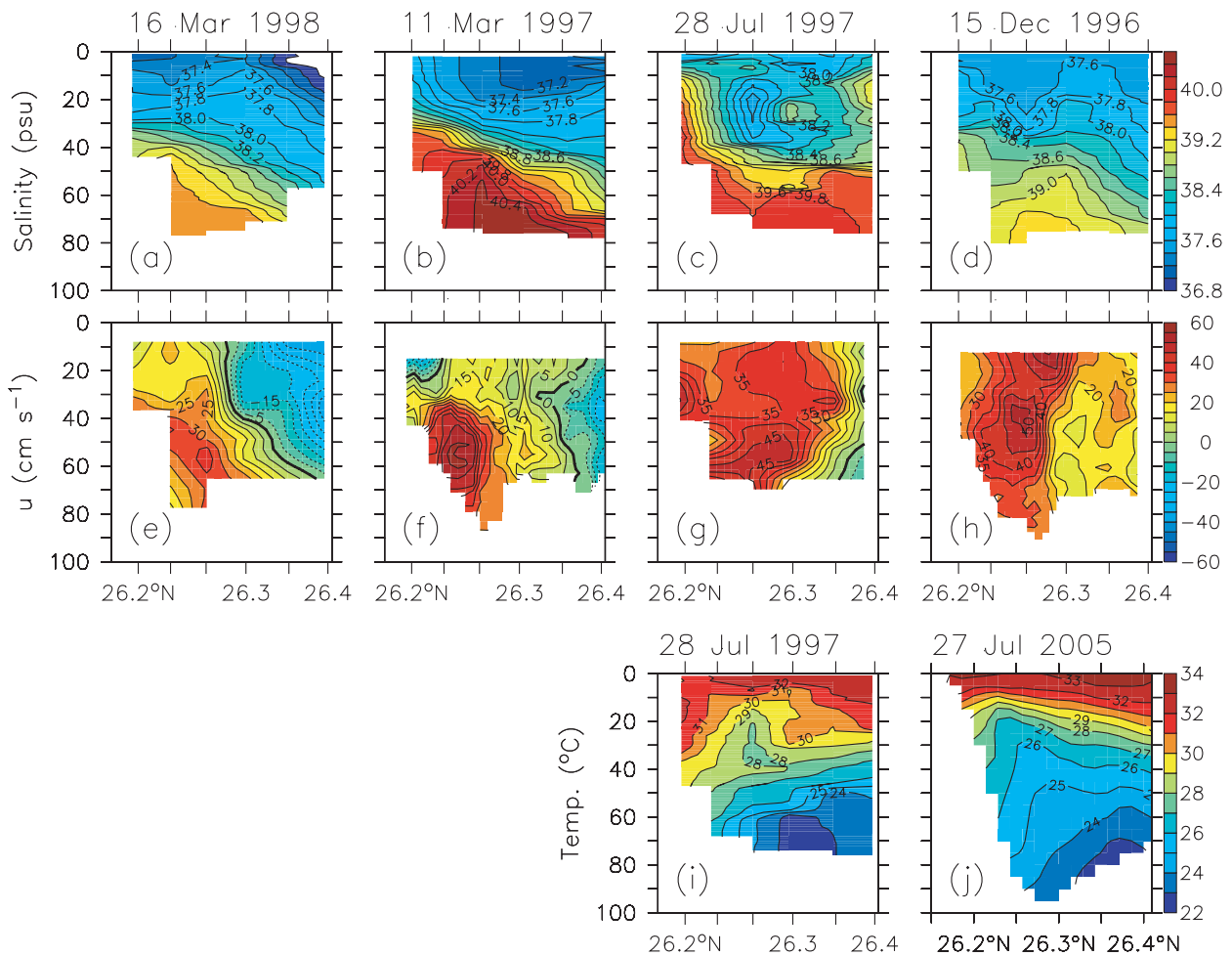
FIG. 6. Cross sections of (a)–(d) salinity and (e)–(h) detided along-strait (055°T) velocity (cm s^{-1}) from the observations of Johns et al. (2003) for 16 Mar 1998, 11 Mar 1997, 28 Jul 1997, and 15 Dec 1996. Cross sections of temperature (°C) from (i) the observations during 28 Jul 1997 and (j) the model during 27 Jul 2005. The model temperature is extracted along the observed locations. The observational latitude values corresponding to tic marks are 26.2°, 26.24°, 26.27°, 26.30°, 26.35°, and 26.4°N. The hydrographic stations occupied in the southern strait during these periods are indicated by the solid line in Fig. 7j.

(2003) noted a small wedge of inflow (upper 30 m) along the southern part of the channel from their 11 March 1997 survey (Fig. 6f). Model currents do indicate several such short-term current reversals, especially during March–June. The along-strait velocity during 14 March 2005 (Fig. 7f) shows a small wedge of inflow along the southern side of the channel that is more pronounced slightly southwest of the survey track in Fig. 7j.

The existence of this short-term flow reversal is also verified from independent drifter data during March 2003 provided by the Naval Oceanographic Office. A snapshot of the model currents in the upper 20 m for 2 and 7 March 2003, superimposed on the drifter trajectory during March 2003, is depicted in Fig. 8. Though the drifter was located farther away (southwest) from the strait, the changes in the circulation reflected the

entire stretch of the coastal area. Between 1 and 2 March, the drifter moved from 24.78°N, 54.2°E to 24.95°N, 54.58°E (red line in Fig. 8b), suggesting a northeastward current consistent with the model flow (Fig. 8a). The drifter then moved in a southwestward direction between 2 and 8 March (from 24.95°N, 54.58°E to 24.74°N, 54.18°E; green line in Fig. 8b), also in agreement with the model currents. This appears to be an indication of surface currents being influenced by the frequent changes in the wind direction.

Although the surface currents seem to be exhibiting a typical inflow–outflow exchange circulation pattern through the strait, a closer look at the currents in the upper 40 m (Figs. 7i and 7j) reveals a cyclonic recirculation cell. A large part of the inflow that enters the Persian Gulf through the northern side of the strait
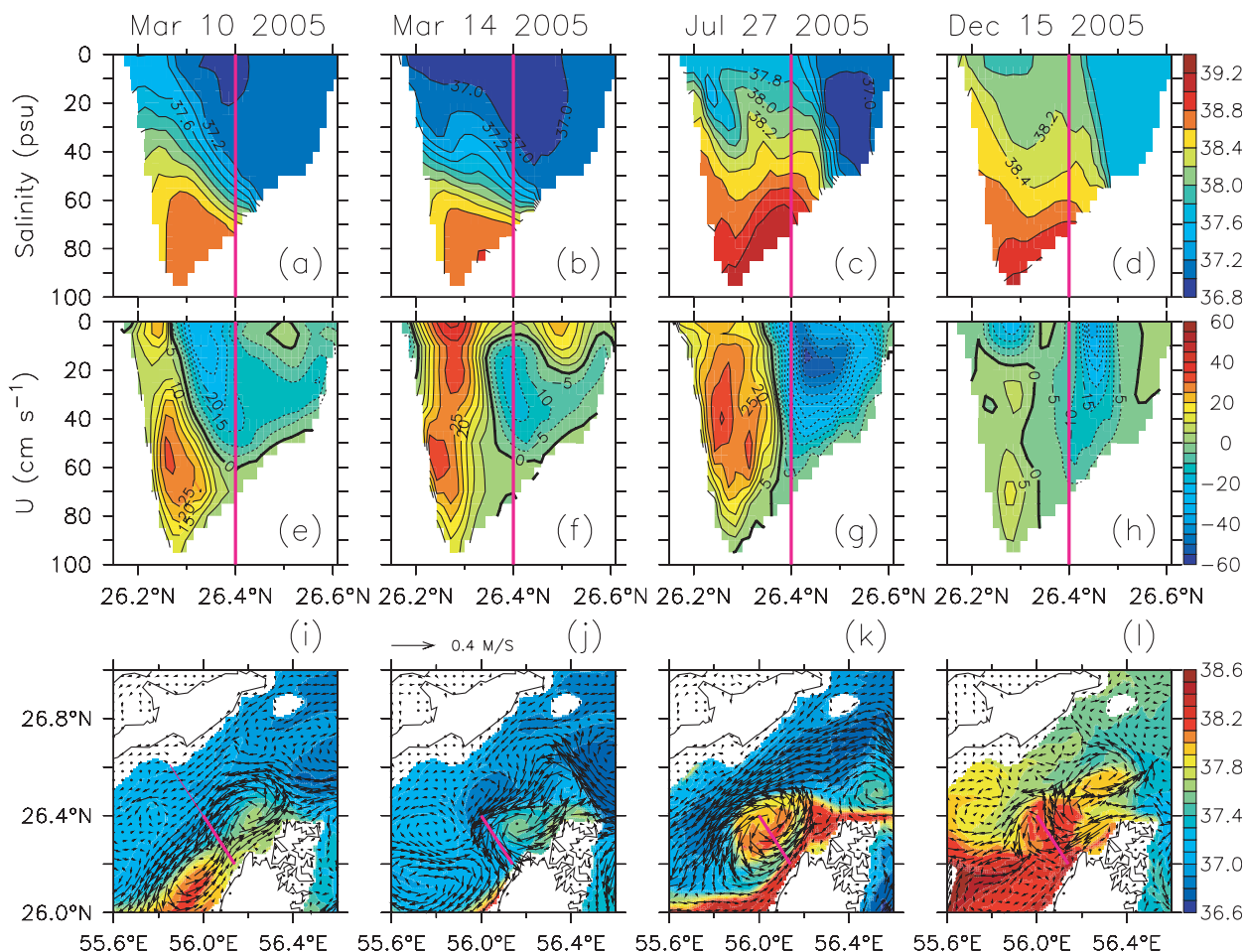
FIG. 7. Cross sections of (a)–(d) salinity and (e)–(h) along-strait velocity along the section indicated by the solid line in (i) from the model during 10 and 14 Mar, 27 Jul, and 15 Dec 2005. (i)–(l) Snapshots of currents in the upper 40 m superimposed on the salinity at 20 m for the same periods. The periods of these sections correspond to the observations of Johns et al. (2003), but for a different year. The vertical lines in (a)–(h) mark the northern end of the observational location (26.2°–26.4°N), which is indicated by the solid line in (j). It should be noted that the Johns et al. (2003) sections extended only ~32 km across the southern part of the Strait of Hormuz. The contour interval for salinity is 0.2 psu and for velocity it is 5 cm s^{-1} with solid (dashed) velocity contours for eastward (westward) flow.

turns offshore and becomes part of the outflow approximately between 56° and 56.1°E (Fig. 7j). Also, the outflow that leaves the western side of the strait becomes part of a recirculation that actually closes off within the strait at about 56.4°E (Musandem Peninsula). A possible explanation, also suggested by Johns et al. (2003), is that the sharp bend in the strait at the Musandem Peninsula, where the shallow inflow from the Gulf of Oman is forced to turn more than 90° as it enters the Persian Gulf, could lead to such a recirculation in the lee of the peninsula. While this appears to be a consistent feature in Fig. 5, the existence of this recirculation needs to be verified against observations.

An intriguing feature of the observed salinity during 28 July 1997 was a patch of low-salinity water (38 psu) sandwiched between slightly saltier water (38–39.8 psu) in the upper 40 m (Fig. 6c). This low-salinity water contrasted with the along-strait velocity, which indicated a strong outflow of 35 cm s^{-1} (Fig. 6g). Furthermore, the presence of somewhat saltier water in the northern end of the section (~26.4°N) contrasted with a weak inflow of ~5 cm s^{-1}. The temperature section during this period indicated a thermal dome in the upper 40 m (26.27°N; Fig. 6i) coincident with a patch of low-salinity water. The 29°C isotherm, for instance, moved from 50 m at 26.2°N to 20 m at about 26.27°N. The vertical doming of isotherms suggests a cyclonic eddy. It is interesting to note that the simulated salinity, along-strait velocity (Figs. 7c and 7g), and temperature (Fig. 6j) during 27 July 2005 do show similar characteristics of the observed features; a patch of low-salinity water (37.8 psu), an outflow of 30 cm s^{-1}, and a weak thermal dome.
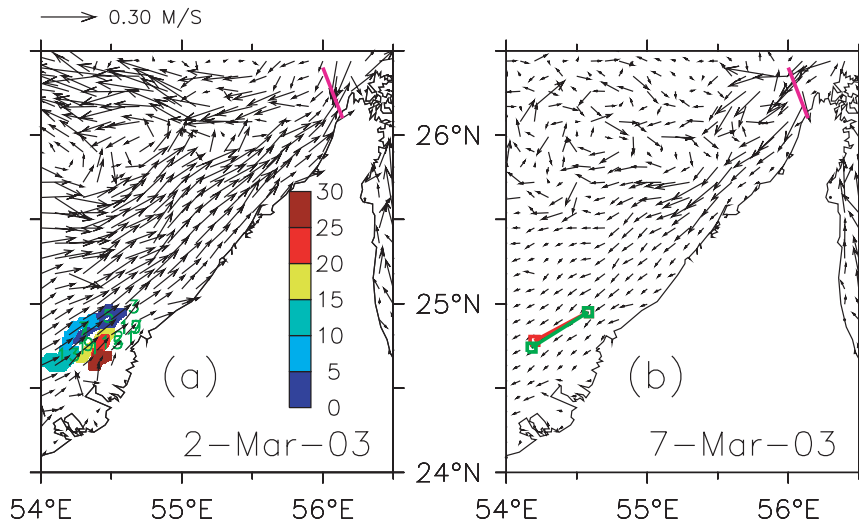
FIG. 8. Comparisons of model currents with the trajectories of a drifter during (a) 2 Mar and (b) 7 Mar 2003. Shading indicates the day between 1 and 30 Mar 2003. Between 1 and 2 Mar, the drifter moved from 24.78°N, 54.2°E to 24.95°N, 54.58°E [red line in (b)] and between 2 and 8 Mar, the drifter moved from 24.95°N, 54.58°E to 24.74°N, 54.18°E [green line in (b)]. This short-term reversal of the circulation (which is also true for the southern part of the strait) is consistent with the model currents.

Model currents in the upper 40 m overlaid on the salinity at 20 m (Fig. 7k) reveal a cyclonic eddy, and the associated salinity distribution explains the conspicuous characteristics of the salinity in Fig. 7c. A small band of saltier water exits the strait along the southern side of the channel as evidenced by both the model and the observations. The surface inflow that carries less saline water from the Gulf of Oman into the Persian Gulf along the northern part of the strait bifurcates at about 56°E, with one branch continuing northwestward along the Iranian coast and the other branch turns south to form a cyclonic eddy. Thus, the patch of less saline water that appears north of a small band of saltier water has its origin in the Gulf of Oman and marks the southern flank of the cyclonic eddy. As we will discuss in section 3c, the eddy formation occurs farther upstream in the strait where less saline water overlays the saltier PGW. The offshore veering of the fresher inflow in turn encircles the saltier PGW, which leads to the formation of a high-salinity eddy core surrounded by a low-salinity ring (Fig. 7k). In addition, the high-salinity area within the eddy core is maintained owing to the increasing salinity with depth. From the similarities between the model and the observed salinity in Figs. 6c and 7c, we can see that the Johns et al. (2003) hydrographic section during 28 July 1997 transited part of the cyclonic eddy core. It should be noted that the cyclonic eddy has a very weak signature at the surface salinity.

While the observed core of the maximum outflow occurred at deeper depths during March 1997 and 1998 (50 and 30 cm s^{-1}, respectively), a surface-intensified outflow (40–50 cm s^{-1}) overlying the weak deeper outflow was evident during 15 December 1996 (Fig. 6h). The core of the outflow, however, contrasted with the lowest salinity of 37.6 psu (Fig. 6d) in the upper 40 m with slightly saltier water in the north. This salinity distribution, like that during 28 July 1997, was most probably the result of the returning flow from the north. However, the model salinity and along-strait velocity during 15 December 2005 are significantly different and weaker than in the observations (Figs. 7d and 7h). Furthermore, the surface currents do not indicate a well-defined cyclonic eddy (Fig. 7l).

Further evidence of the existence of a cyclonic eddy in the Strait of Hormuz comes from the high-resolution (~1 km) MODIS SST imagery. Daily snapshots of SST during 12 and 20 July, 25 August, and 26 September 2005 are depicted in Fig. 9. Snapshots of the model temperature at 20 m with overlaid currents in the upper 40 m for the same period are also included. MODIS SST during 12 July reveals a cyclonic eddy located between 55° and 56°E, in conformity with the model. The periphery of the eddy is clearly characterized by warm PGW water. It is interesting to note that the warmer PGW water leaving the gulf is surrounded by the cooler water entering the strait from the region east of the Musandem Peninsula. The signature of this eddy is weak during 20 July 2005. Another instance indicating the passage of a cyclonic eddy through the strait can be inferred from MODIS SSTs during 25 August 2005
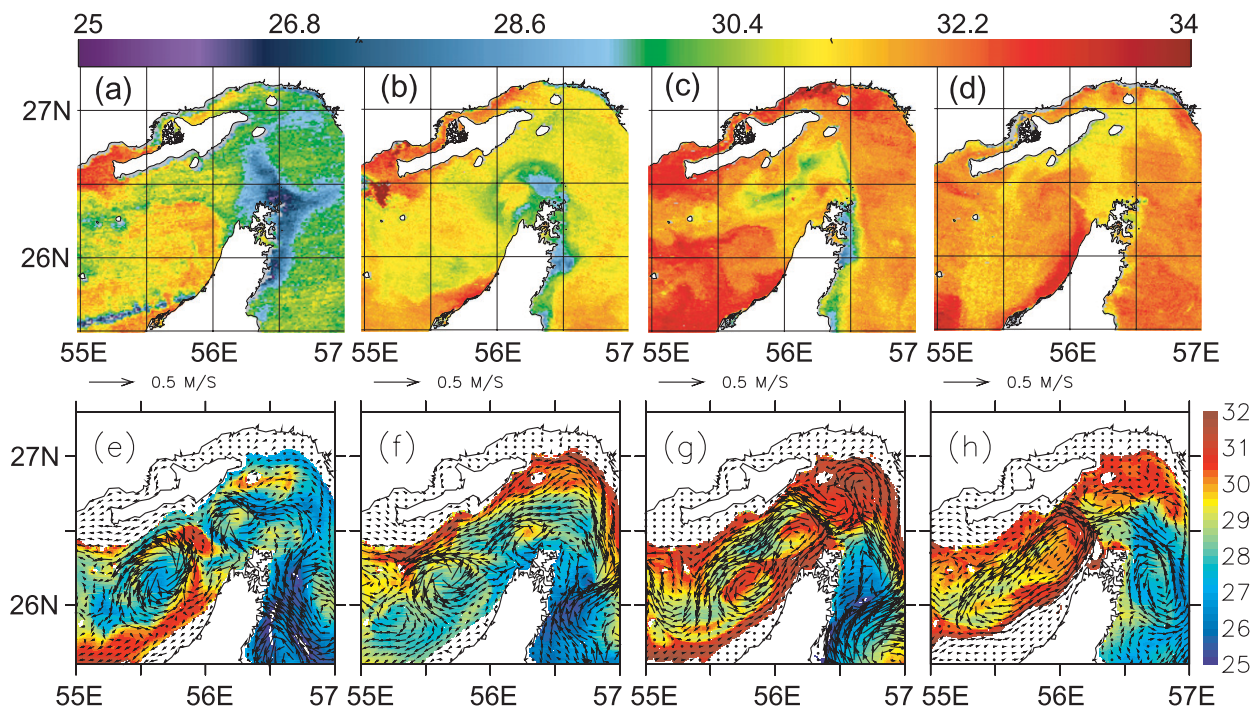
FIG. 9. MODIS (~1 km) SST imagery during (a) 12 Jul and (b) 20 Jul, (c) 25 Aug, and (d) 26 Sep 2005 and (e)–(h) model temperatures at 20 m with overlaid currents in the upper 40 m for the same period. Model temperature at 20 m is shown because the eddy has a weaker signature at the surface than at the subsurface owing to the strong near-surface stratification.

(Fig. 9c), which have a temperature pattern that is similar to that described previously. The model temperature and velocity characterize such an eddy: warm PGW within the core while propagating downstream (Fig. 9g). The cooler water inflow from the region east of Musandem Peninsula delineates the northern flank of the cyclonic eddy, matching well with the observed SST pattern. The location of the eastern terminus of the cyclonic eddy on 26 September is clearly visible both in the model and MODIS SST maps. It should be noted that the eddy has a stronger subsurface signature relative to the surface due to the strong near-surface stratification. The passage of cyclonic eddies during these periods is also reflected in the salinity at 40-m depth (Fig. 11).

A consistent picture emerging from the above analysis is that part of the inflow and outflow through the Strait of Hormuz forms a recirculation cell that closes off within the strait. The location of its western terminus is determined by the sill and channels, while the sharp bend in the strait at the Musandem Peninsula marks the eastern end. The offshore turning of the fresher inflow at the western terminus generates cyclonic eddies that, in turn, propagate downstream. The exchange circulation through the Strait of Hormuz, unlike major outflows in other regions, consists of a relatively fresh in-

flow at the northern part of the strait, and a saline deep outflow in the southern part of the strait with occasional fresh, surface inflow in spring. This suggests a more complex exchange circulation through the Strait of Hormuz than has previously been reported.

b. Observed and simulated variation of salinity outflow

A time series of temperature, salinity, zonal velocity (u), and meridional velocity (v) from a mooring at 26.26°N, 56.08°E collected during 1997 (Johns et al. 2003) is compared with the model fields during 2005 (Fig. 10). Both the model and observations depict an annual cycle in temperature. Observed maximum and minimum temperatures occurred during October (~33°C) and February (~20°C). The annual cycle of temperature undergoes a period of cooling during winter (December–February) when convective mixing produces a weakly stratified vertically mixed water column and a period of warming in summer (June–October). The development of a strongly stratified upper ocean starts in April–May when the ocean begins to gain heat from the atmosphere. The deepening of the mixed layer and the erosion of the thermocline occur when the upper ocean begins to lose heat in November. A major difference between the model and the observations during the
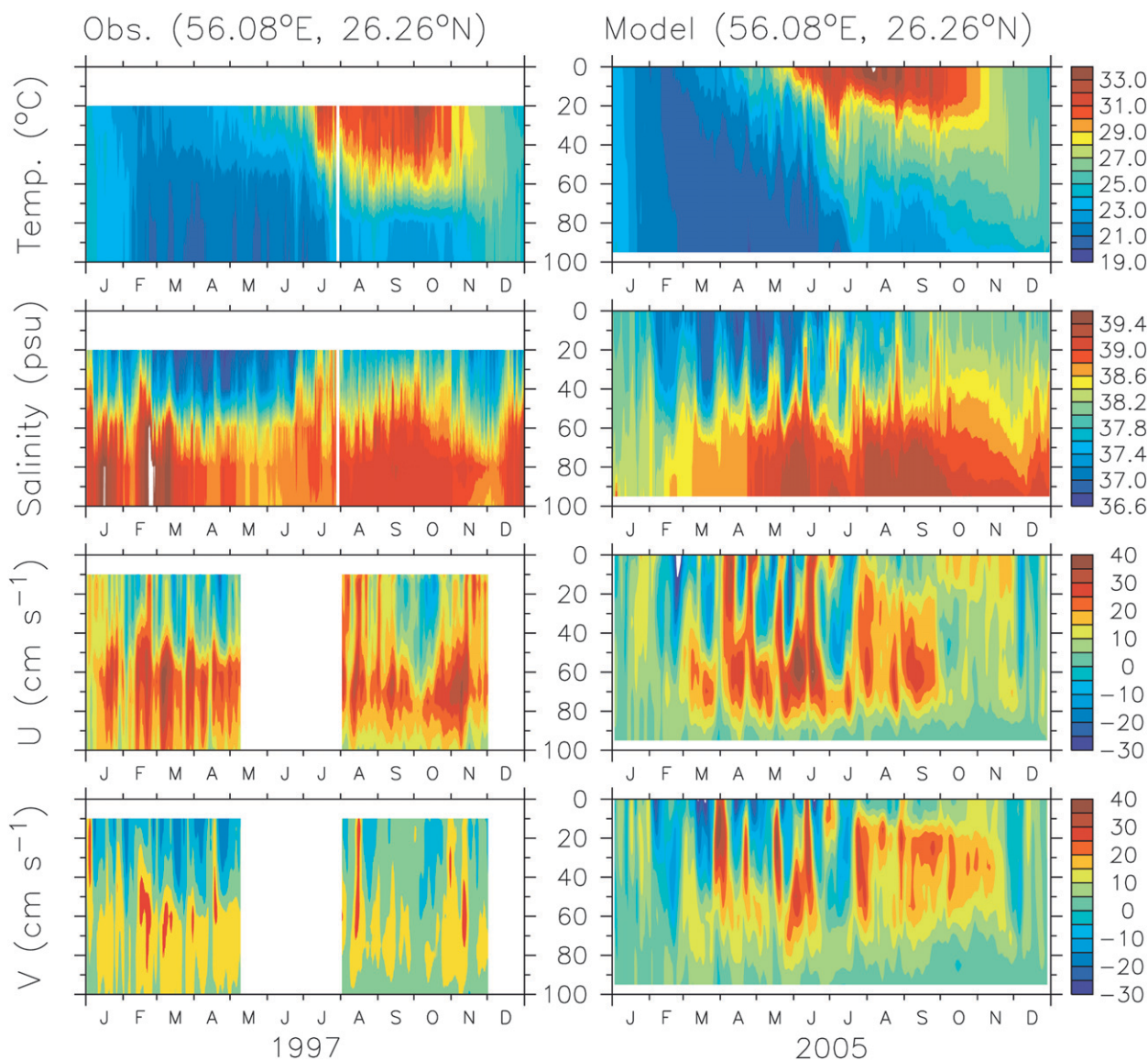
FIG. 10. Time series of temperature, salinity, zonal velocity (u), and meridional velocity (v) in the Strait of Hormuz (26.26°N, 56.08°E) from (left) observations during 1997 (Johns et al. 2003) and (right) the model during 2005. Daily snapshots of model fields are used. The observed temperature, salinity, and velocity fields are sampled at 30 s. Temperature and salinity fields are applied with 1-day window Parzen smoothing, and 5-day smoothing is applied for velocities. Velocity data are missing between early May and early August, and during December 1997 (see Johns et al. 2003 for details). The model salinity scaling is adjusted (maximum salinity is set to 39.6, which is 1 psu less than that in the observations) to highlight the high-salinity events.

summer season is that the observations indicate a deeper summertime (July–October 1997) mixed layer depth (~50 m), suggesting enhanced vertical mixing while the model mixed layer depth deepens only to ~20 m. This model–data discrepancy could come from (at least) two sources: 1) interannual variability, because the model is not forced with the same conditions that produced the observed fields, and 2) a lack of tidal mixing in the model, which may have played an important role in mixing at the strait.

The agreement between the simulated and observed salinity variabilities is fairly good except that the model deep outflow salinity is fresher than the observations by 1 psu. Salinity variability in the strait, unlike for temperature, shows a weak annual cycle. The outflow of high-salinity water (>39 psu) peaks in summer and weakens in winter. The inflow of low-salinity water (~37 psu) from the Gulf of Oman dominates the upper 50 m during February–June, which is consistent with the observations. The outflow of high salinity is marginally

stronger from mid-July to October both in the observations and the model. The highest simulated salinity (39.6 psu) is fresher than that in the observations (40.6 psu) by 1 psu because of the relaxation to the GDEM climatology. The model also failed to produce the saltier deep-water outflow that is seen in the observations during January–March 1997.

The most striking feature is the episodic variation in the salinity in- and outflows. There are pulselike events of high salinity in both the observations and the model throughout the period, but predominantly between February and July. A clear signature of these events also can best be seen in several of the figures (e.g., Figs. 3, 11, 14, and 16), where the salinity at 40-m depth is plotted. Six such dominant events are seen in the model at ~40 m, each characterized by a rapid increase in salinity followed by an abrupt decline (Fig. 14a). The salinity increases from approximately 37 to 38.5 psu during each event, a 1–1.5-psu increase, and it often reaches up to 2.5 psu in the observations (Fig. 13a). These events are separated between 15 and 30 days in both the observations and the simulation. Although the episodic pulses are persistent in both years (1997 and 2005), the different times of the occurrences suggest that there is considerable interannual variability (also see Fig. 3). The signatures of these episodic events are less apparent in the temperature distribution in part due to the weakly stratified upper ocean.

The salinity events are characterized by strong coherence between the enhanced flows in both the zonal and meridional directions. A time series of zonal and meridional velocities measured by the moored ADCPs and near-bottom current meters (Johns et al. 2003), and obtained from the model, are shown in Fig. 10. During the episodic pulses, zonal flows reverse and accelerate to speeds of 20–30 cm s^{-1} and often reach the bottom. These flow events closely correspond to the salinity fluctuations. The maximum speeds of the outflow (~30 cm s^{-1}) in both the model and observations occur at ~60 m (Johns et al. 2003). The meridional flows show similar episodic variations in magnitude and direction, consistent with observations. The flow is generally directed to the southwest or northeast. There is an indication in the model currents that suggests a seasonality in the outflow as having stronger currents during April–September and weaker currents in the winter. Such seasonality could not be inferred from the observations due to the lack of data during May–July. The model velocity, however, has two major differences: 1) the model outflow is weaker than the observations during October–February and 2) the model outflow does not extend to the bottom as in the observations.

The spatial and temporal evolutions of the salinity events can best be seen from the snapshots of salinity at 40 m for every 15 days shown in Fig. 11. It is clear that the large-amplitude fluctuations in the salinity outflow at the observations site are collected at varying phases of the passage of the cyclonic eddies. For example, passage of a cyclonic eddy at 26.26°N, 56.08°E during early April accompanies enhanced zonal flows and a sharp increase in salinity (Fig. 10). These cyclones appear to form rather abruptly in the vicinity of 26°N, 55.5°E, where the low-salinity inflow encounters the high-salinity outflow. Subsequently, these eddies move northeast toward the strait and become less distinguishable farther downstream. Although generation and propagation of these eddies are evident throughout the year, they are more pronounced during the spring and summer months. During this period, the low-salinity inflow is stronger and results in a marked variation in the degree of stratification and the strength of the horizontal salinity gradient across the strait. As the inflow of low-salinity water decreases during fall and winter, the strength of the cross-channel (north–south) salinity front weakens and, consequently, the high-salinity outflow fills the strait. Therefore, the salinity events are less discernable.

An intriguing impression arising from the salinity maps is that the eddy formation occurs in the vicinity of 26°N, 55.5°E, and occurs somewhat continuously. However, why is there such a preferred location for the eddy's formation? An examination of the circulation in the strait (Figs. 5 and 12) provides some clues as to the underlying process. The dominant circulation in the strait consists of a cyclonic recirculation cell. The western extent of the cell lies in the vicinity of 55°–55.5°E. Part of the inflow entering the Persian Gulf along the northern part of the strait subsequently turns offshore (seaward) between 55° and 55.5°E and converges with the outflow. This circulation pattern persists throughout the year but is less apparent during the period of weaker circulation during winter. This offshore current therefore provides an ideal location for cyclonic eddies to develop and evolve (Figs. 12a and 12b). The offshore current can be the result of one or several sources in combination, with likely candidates being the channel bends, varying bathymetry (such as sills), and persistent lateral density gradients. The bathymetry of the strait is highly variable (Fig. 1) in the direction of the flow. The deepest part of the channel (80-m isobaths in Fig. 1) is separated by a sill at ~55.4°E. The sill depth is about 40–60 m. Furthermore, most of the surface inflow at this location is constrained by the elevated ridges (>40 m depth) and narrower channel width (60-m isobaths in Fig. 1). This, together with a strong lateral density gradient, qualifies this region as being the most relevant to the eddy formation process.
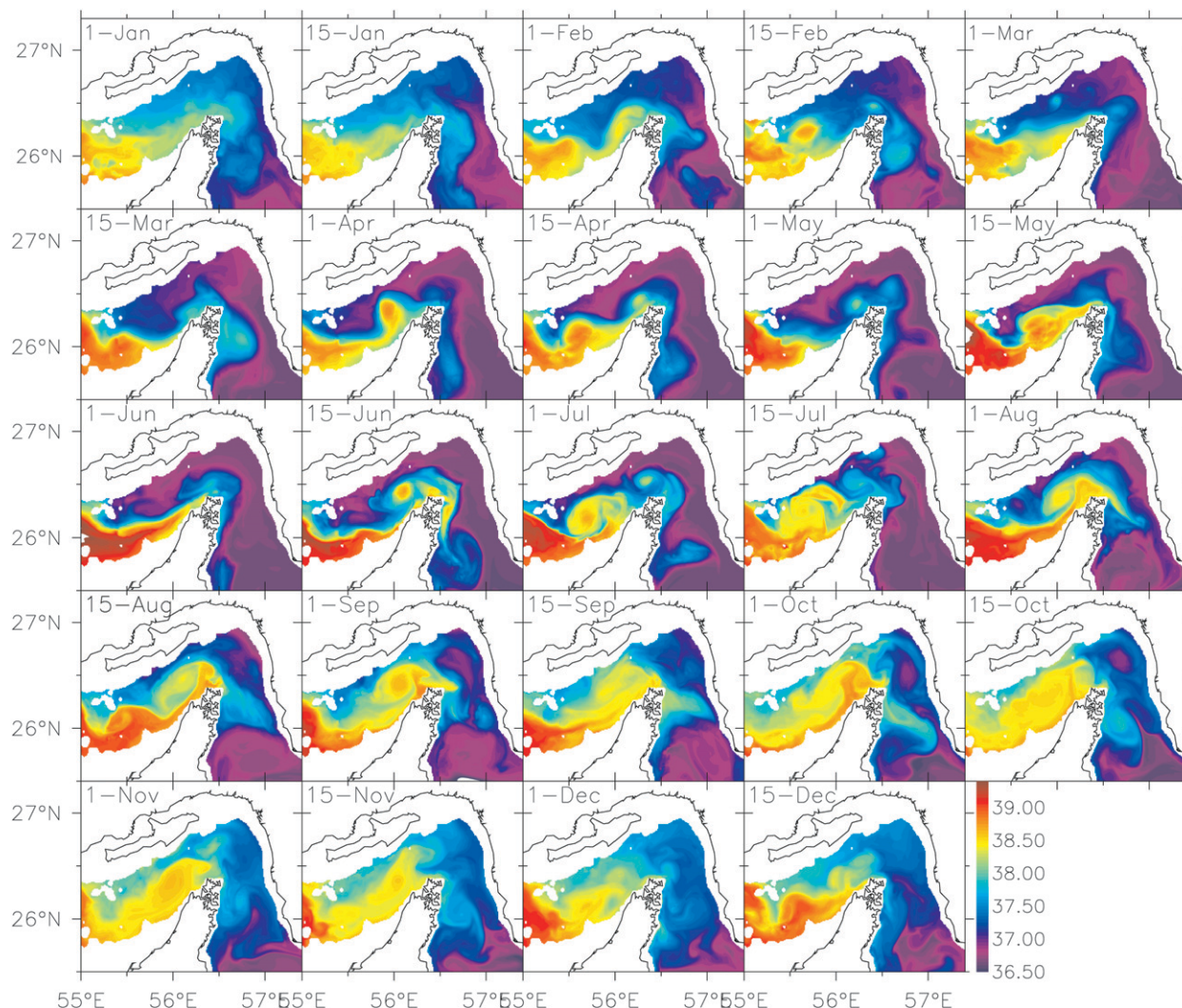
FIG. 11. Daily snapshots of model salinity at 40 m for every 15-day interval during 2005. The onset of cyclonic eddies and their downstream propagation are evident throughout the year. High-salinity PGW is entrained into the eddy cores.

After formation, the cyclonic eddies move northeast toward the strait (downstream) approximately following the deepest part of the channel. The location of an eddy center was traced for every 5 days between 20 March and 20 April (indicated by white squares in Fig. 12a), from which a translation speed of 4.1 cm s^{-1} (3.5 km day^{-1}) was obtained. The average diameter of the eddy is about 62 km near the formation region and decreases in the downstream direction. Eddies have a signature of Persian Gulf water in their cores and have swirl velocities of 30–40 cm s^{-1}, which is greater than the surrounding mean flow by roughly 10–20 cm s^{-1}. Interestingly, the cyclonic eddy that is present during 10 April 2005 (Fig. 12a) is also captured by the MODIS-derived surface chlorophyll during 1 April 2005 (Fig. 12e). This cyclonic eddy is clearly indicated by an area of low-

level chlorophyll concentration centered around 26°N, 55.5°E (Fig. 12e), comparing well to the model eddy.

c. Mechanisms of high-salinity events

While an instantaneous view of the velocity and salinity fields elucidates the structure of the mesoscale eddies that give rise to variability in the salinity outflow, a key issue remaining to be answered is, what are the underlying processes generating these eddies? We interpret the mechanisms of eddy formation to be the result of variable exchange circulation through the strait and its associated instabilities. Abrupt changes in the exchange circulation can be induced by changes in wind stress forcing. To demonstrate this, we first examine the vector–stick plot of basin-averaged (west of 56°E) wind velocity components obtained from the 6-hourly National
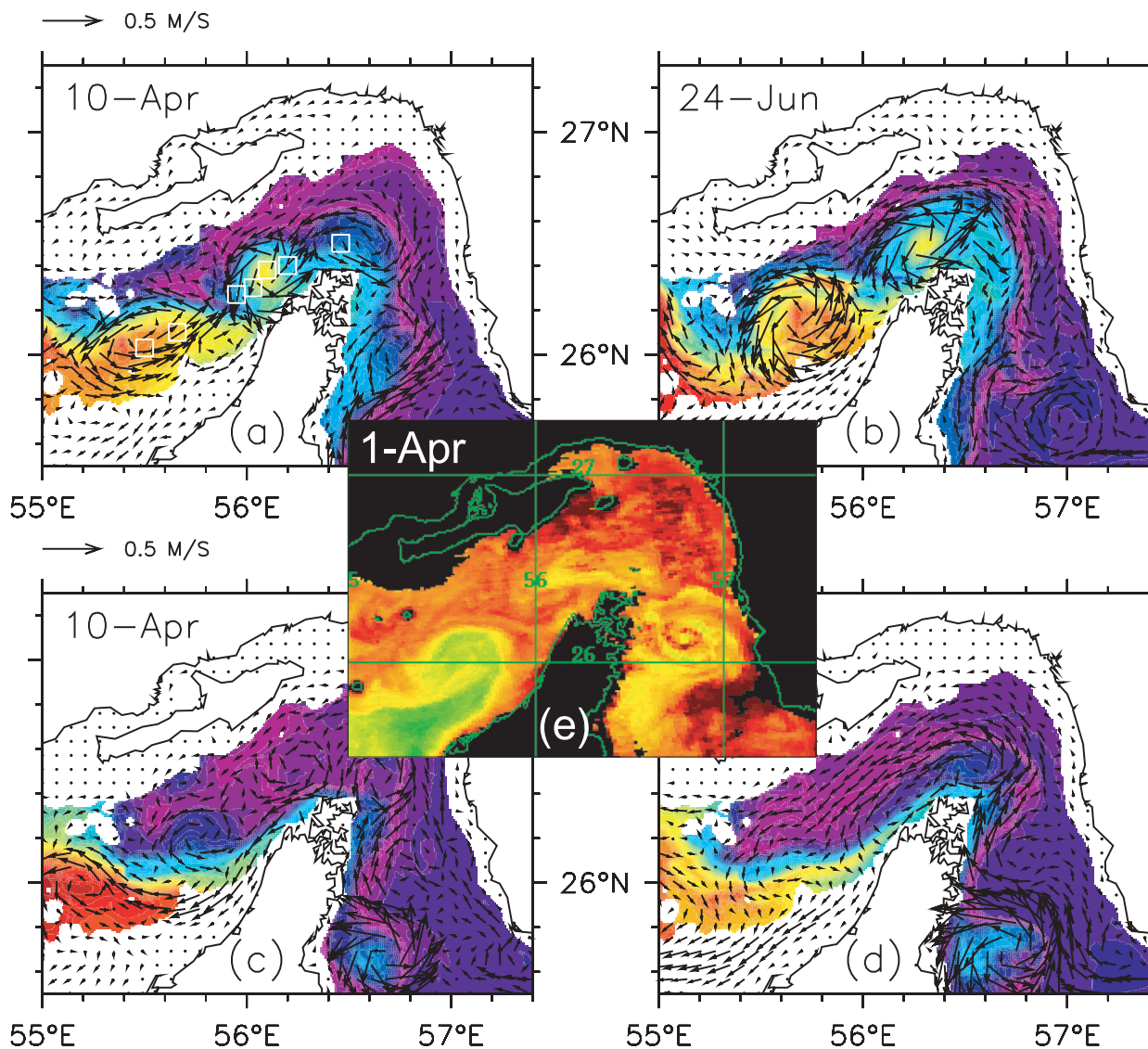
FIG. 12. (a),(b) Currents in the upper 40 m (average of upper 40 m) superimposed on the salinity at 40 m during 10 Apr and 24 Jun 2005 from the control run. The cyclonic eddies form in the vicinity of 26°N, 55.5°E, where the inflow turns offshore and subsequently joins the outflow circulation. Temporal locations of eddy centers are marked with squares for every 5-day interval between 20 Mar and 20 Apr 2005. The average translation speed of the eddy is about 4.1 cm s^{-1}. (c),(d) Same as in (a),(b) but from the simulation without wind stress forcing (see section 3c). (e) MODIS-derived surface chlorophyll during 1 Apr 2005, indicating a cyclonic eddy centered around 26°N, 55.5°E, conforming well to the model eddy during 10 Apr 2005.

Centers for Environmental Prediction–Department of Energy (NCEP–DOE) reanalysis product matching with the moored observation period of 1997–98 (Johns et al. 2003) and the observed salinity at 40 m (salinity events are well pronounced at this depth) in Fig. 13a. Apart from the seasonal variability, the salinity fluctuations associated with the variable outflow in the strait are the dominant signal. The amplitudes of these events often reach ~2 psu, which is nearly the same as the magnitude of the seasonal cycle. The time scales of these salinity events range from 15 to 30 days on average.

A comparison of these salinity events (marked by arrows) with the surface wind velocity clearly suggests that the period of strong salinity outflow coincides with the synoptic variability in the wind field. The winds in the Persian Gulf region are highly variable, changing from northwesterly to southeasterly at a period of several days to a few weeks, roughly agreeing with the frequency of the salinity events. On the other hand, during July–September 1997, the winds are less variable and northwesterly. Consequently, the salinity events are not discernable. A comparison of winds during 2005–06
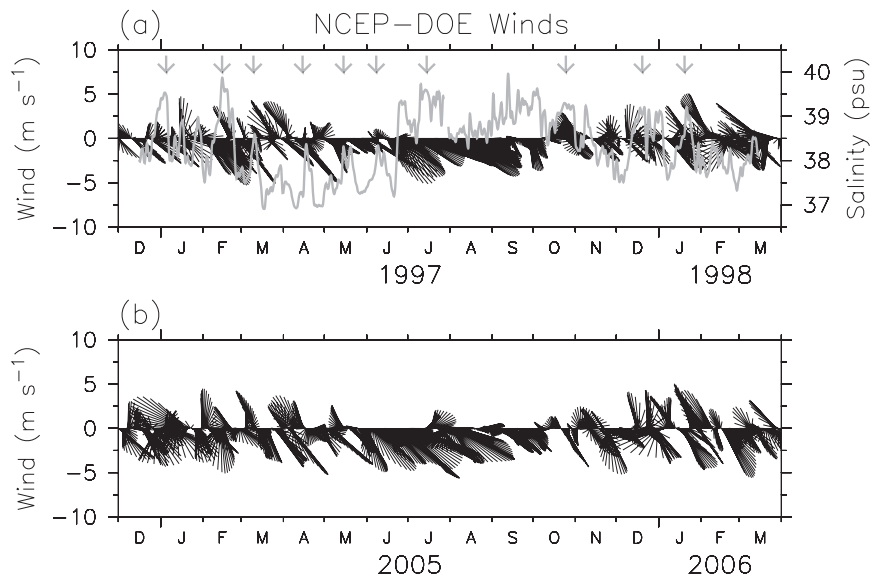
FIG. 13. (a) Stick plot of NCEP–DOE reanalysis wind velocity vectors averaged over the Persian Gulf region (west of 56°E) and the observed salinity at 40 m in the Strait of Hormuz [26.26°N, 56.08°E; Johns et al. (2003)] during December 1996–March 1998 (gray line). Salinity is sampled at 30 s and winds are available for 6-h intervals. A 2-day Parzen smoothing is applied to the salinity to highlight the episodic variations in the high-salinity outflow. Arrows mark periods of increased salinity outflow events. (b) The same wind vectors as in (a) but for the period 2004–06.

(Fig. 13b) essentially shows similar high-frequency variations consistent with 1997–98 periods. However, the details of wind fluctuations show significant differences that do seem to have a bearing on the salinity outflow events. Again, winds are from the northwest and exhibit little variability during June–September 2005.

We now examine the variability in wind stress forcing (model forcing) and the simulated salinity outflow in 2005. The spatial average (west of 56°E) of wind stress vectors obtained from the ½° NOGAPS atmospheric product and the simulated salinity at 40 m at the mooring site (26.26°N, 56.08°E) is shown in Fig. 14a. The corresponding wind fields derived from the QuikSCAT are included for comparison (Fig. 14b). In general, the comparison demonstrates that the NOGAPS winds are in close agreement with the QuikSCAT winds—in particular, the shift from northwesterly winds to southeasterly winds during winter. The QuikSCAT winds are not daily averages, rather they are 3-day moving averages, so it comes as no surprise that some high-frequency wind events are filtered out. Generally, the overall wind blows predominantly northwesterly throughout the year—strongly during winter and spring and weakly during summer.

The magnitude and direction of the wind stress are highly variable from early winter to June and relatively calm during the rest of the year. The salinity (Fig. 14a) shows several strong events during the simulation period. Six distinct events are evident, each characterized by a rapid increase in salinity followed by an abrupt decline. In accordance with the observations (Fig. 13a), the amplitudes of these salinity events often reach 1.0–1.5 psu and they occur between the winter and summer months. Salinity is much less variable between July and December, and as a consequence no strong events are apparent. The associated wind-driven current fluctuations in the strait are presented in Fig. 14c. Current and salinity fluctuations tend to be coherent with the wind stress forcing in the Persian Gulf. This again reinforces the fact that fluctuations in the wind stress forcing drive salinity variability in the strait through the production of mesoscale cyclonic eddies. Furthermore, comparing these results to earlier observations (1997–98) in the same region demonstrates the considerable interannual variability in the salinity outflow.

Since the wind stress forcing is an essential ingredient required for the production of cyclonic eddies and their associated salinity variability, the absence of such forcing is likely to produce no salinity events. To demonstrate this, we performed a model experiment in which the wind stress is set to zero (no Ekman flow) everywhere and kept the wind speed unchanged. By doing so, the heat flux exchange across the air–sea interface remained nearly the same as in the control run and
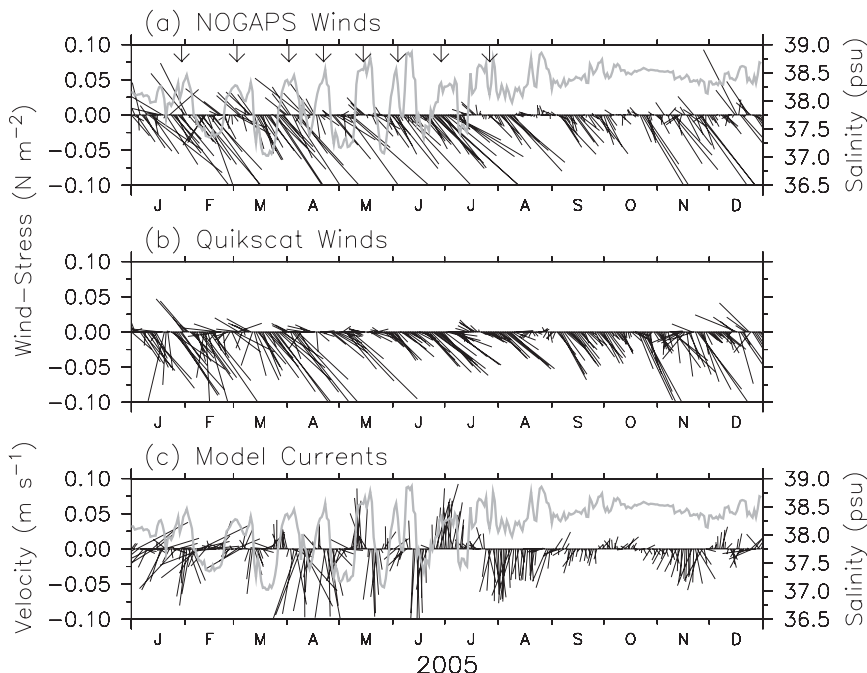
FIG. 14. (a) Stick plot of ½° NOGAPS wind stress averaged for the Persian Gulf region (west of 56°E) and model salinity at 40 m (26.26°N, 56.08°E, gray line) in the Strait of Hormuz during 2005. (b) Stick plot of QuikSCAT wind stress, which is included for comparison. (c) Volume-averaged (26°–27°N, 55.9°–56.4°E, 0–100 m) simulated currents (m s^{-1}) and salinity at 40 m at 26.26°N, 56.08°E. The 3-hourly, ½° NOGAPS wind stress is interpolated to a daily ¼° QuikSCAT grid before averaging. A constant drag coefficient (C_D) value of 1.2×10^{-3} is used to compute the wind stress from the QuikSCAT wind velocity. A daily QuikSCAT wind stress has been generated by taking 3-day moving averages. Eight dominant salinity events are marked by arrows.

hence the rate of PGW formation remained the same. In the absence of the variable Ekman component, the resulting circulation is driven by geostrophy only. The model was run from January to December 2005 using the initial conditions taken from the control run (1 January 2005). A time series of temperature, salinity, and zonal and meridional velocities at the mooring site (26.26°N, 56.08°E) from this experiment is shown in Fig. 15. The absence of wind-driven vertical mixing and current shear at the base of the mixed layer results in a shallower mixed layer and thermocline depths during summer.

A striking difference in the salinity distribution from the control run is the absence of any high-salinity events. This suggests that these spillage events are indeed associated with the changes in the wind stress forcing. It is possible that a weak salinity event seen during February–March may have been generated due to local instability processes or may be the remnants from the control run. The salinity distribution shows a relatively steady near-surface inflow in the upper 60 m and a deep outflow below it. Despite the absence of high-salinity events, the

structure and the amplitude of the salinity outflow are similar to those in the control run. The maximum outflow salinity of 39.4 psu can be seen from mid-July to October. Quite unlike the control run, the zonal–meridional flow is nearly steady and there is no significant variability in the deep outflow (below 50 m). There is some evidence of a variable surface inflow, but it is much weaker than in the control run. As in the control run, the maximum surface inflow (10–20 cm s^{-1}) occurs between March and June. The major conclusion to be drawn is that no cyclones are formed and hence there are no significant episodic variations in the salinity outflow in the absence of a variable Ekman flow. It is also clear that the magnitude of the in- and outflows in the strait are relatively insensitive to wind stress forcing.

However, it is noted that the strongest salinity gradient (hence the density gradient because salinity chiefly controls the density) that occurs farther upstream in the strait (55°–55.5°E) where cyclonic eddies are formed (Figs. 11 and 12a,b) may satisfy the necessary conditions for instability locally even in the absence of a variable Ekman flow. While there is some evidence for eddies in
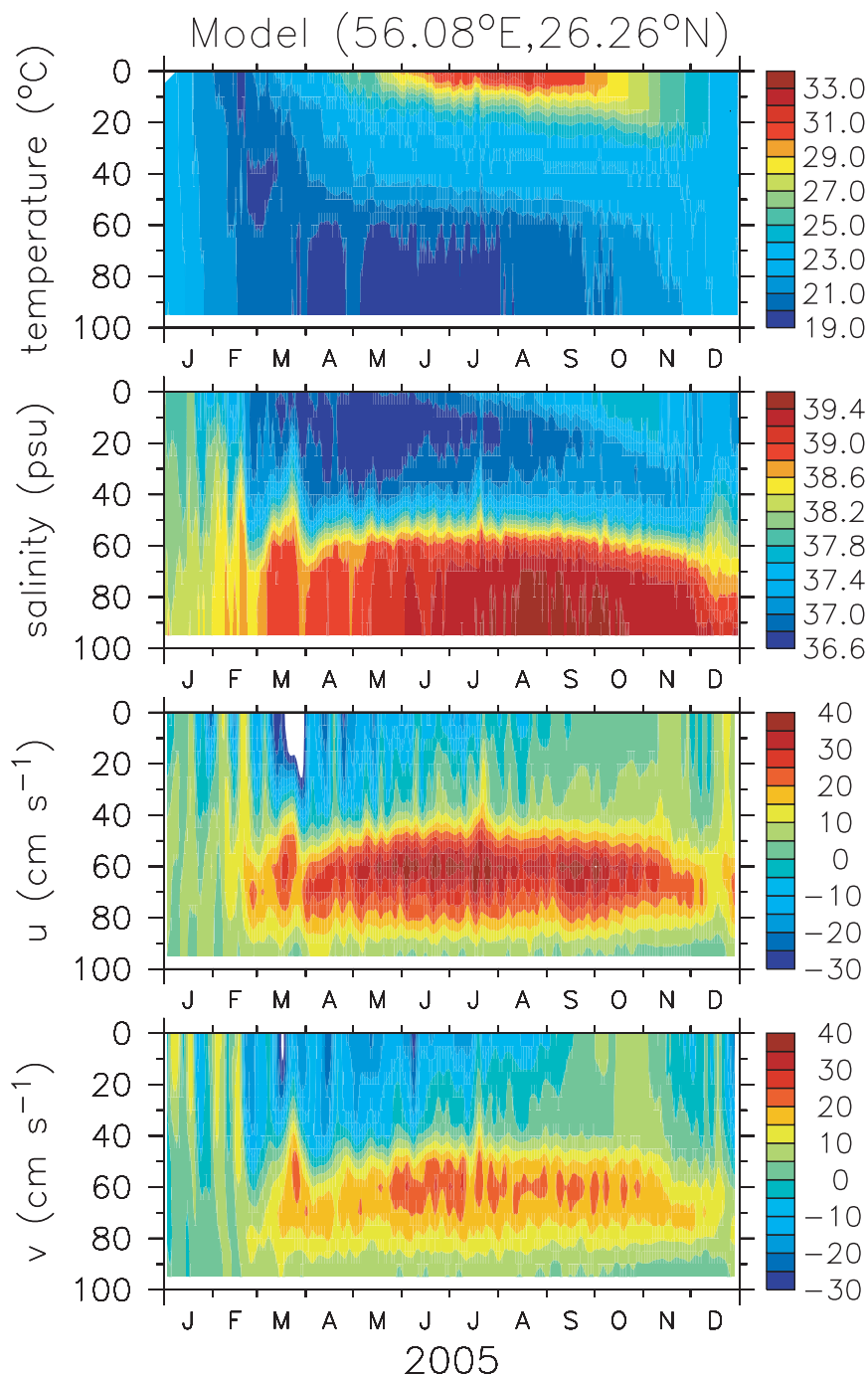
FIG. 15. Same as in Fig. 10, except that the model is run with no wind stress forcing. The wind speed is unchanged from the control run so, as are the air–sea heat fluxes and evaporation. In the absence of the variable Ekman current, the resulting flow is geostrophic. No salinity outflow events are evident.

the simulation without wind stress forcing, their characteristics differ significantly from the control run. Examples of these eddies are shown in Figs. 12c and 12d for 10 April and 24 June. In particular, there is a van-

ishing cyclonic eddy during 10 April (∼26.2°N, 55.8°E) compared to that in the control run (Fig. 12a). An anticyclonic eddy occurs farther downstream on 10 April and no cyclonic eddy is evident west of 56°E during
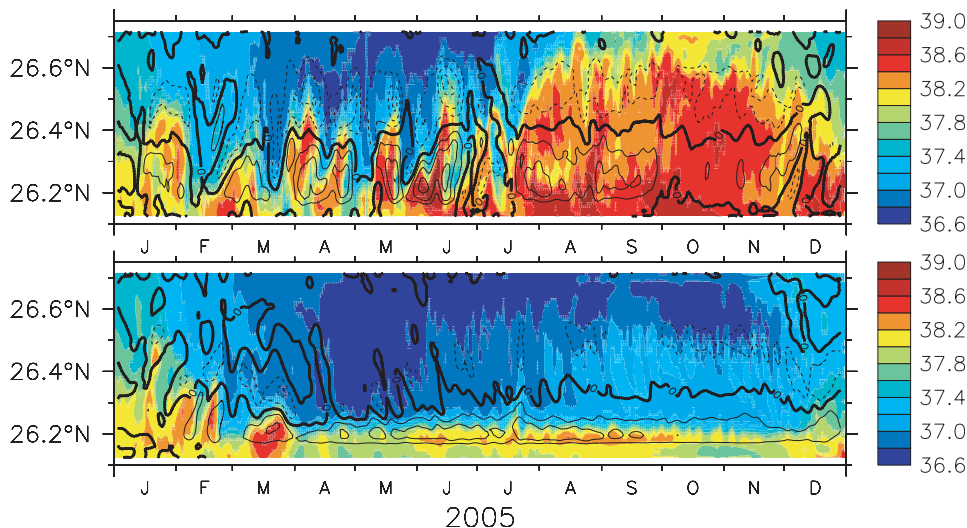
FIG. 16. Time–latitude plot of salinity (shaded) and zonal velocity (contours) at 40 m along 56.08°E from the model run (top) with wind stress forcing (control run) and (bottom) with no wind stress forcing. A 5-day Parzen smoothing is applied to the velocity fields. Positive (negative) velocity values indicate outflow (inflow) through the Strait of Hormuz.

24 June, which is quite different from the control run. This suggests that the strong salinity gradient near the sill (26°N, 55.4°E) is not an essential component of the eddy formation process.

The passage of cyclones through the strait is shown in Fig. 16 as a time–latitude plot of salinity and zonal currents at 40 m along 56.08°E for the control run (top) and the case with no wind stress forcing (bottom). The high-salinity events closely correspond to the periods of enhanced zonal outflows. The meridional extents of these cyclonic eddies are mostly confined to south of ~26.4°N. Unlike in the control run, the zonal flows (and salinity) vary little over time in the absence of variable Ekman currents. Thus, it is clear that cyclogenesis is considerably stronger and more sustained in simulations with wind stress forcing, and that the instability of the exchange circulation through the strait acts to generate mesoscale cyclones near the sill (26°N, 55.5°E), though there may be other sources of mesoscale variability, including the lateral density gradient.

To gain further insight into the nature of the instability mechanism in the eddy generation processes, eddy–mean flow interaction terms are calculated. A calculation of the complete energy budgets is beyond the scope of the present study because the focus is on the eddy generation. For brevity, energy interaction terms involving baroclinic and barotropic instability are discussed. Expressions for the conversions from mean potential to eddy potential energy (T_2) and the effects of the Reynolds stresses on the fluctuating part of the kinetic energy (T_4) are given by Böning and Budich

(1992) in their Eqs. (14) and (16), respectively. Positive values of T_2 suggest the occurrence of baroclinic instability (BCI) and positive T_4 represents barotropic instability (BTI). Figure 17 shows the latitudinal dependence of these terms between 55° and 56°E for the upper 100 m during June 2005. Except for a very small area in the southern flank, values of T_2 are negative, indicating an inverse BCI (i.e., energy transfer occurs from eddy to mean potential energy). Positive values of T_4 in the eddy generation region (26°–26.5°N) indicate BTI owing to the fluctuations in the velocities. This suggests that the barotropic instability of the flow across the Strait of
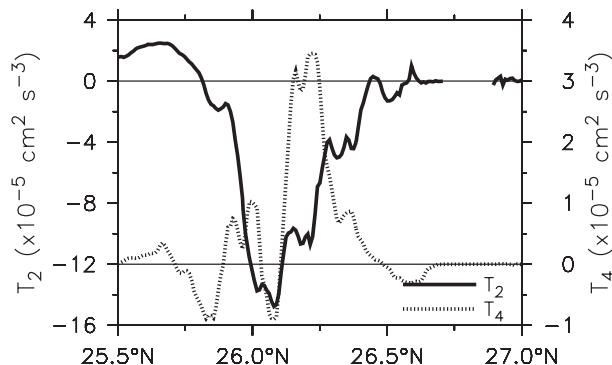

FIG. 17. Latitudinal dependence of the eddy–mean flow interaction terms involving baroclinic (T_2) and barotropic (T_4) instability between 55° and 56°E for the upper 100 m during June 2005. The T_2 and T_4 terms are calculated using the Eqs. (14) and (16) from Boning and Budich (1992), respectively.
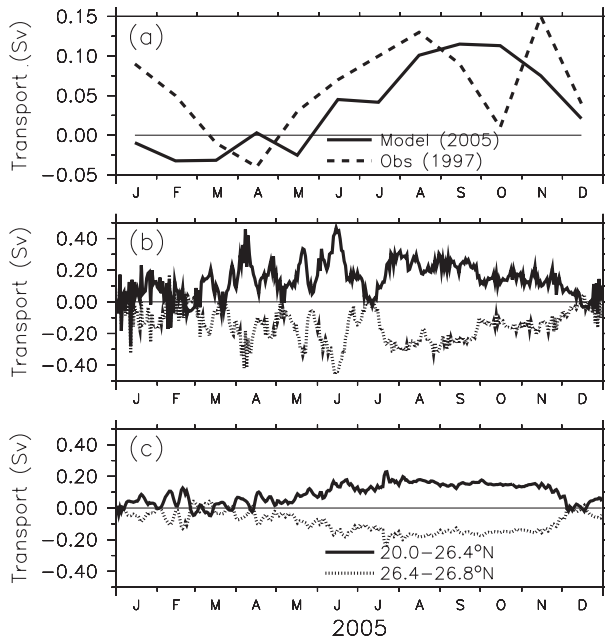
FIG. 18. (a) Comparison of monthly mean values of transport for the upper layer (0–45 m) in the southern part of the strait (26°–26.4°N) from the model during 2005 (solid line) and from the observations during 1997 (dashed line). Note that the observed transport values for the months of June and July are linearly interpolated between the observed values in May and August because of a gap in the current meter records (see Johns et al. 2003 for details). Time series of the transport estimate across the Strait of Hormuz along 56.08°E for the region north of 26.4°N (solid line) and south of 26.4°N (dotted line) from the model run (b) with wind stress forcing (control run) and (c) without wind stress forcing. Units are in Sv. Positive (negative) values indicate outflow (inflow) transport.

Hormuz is the primary excitation mechanism of the eddy by extracting kinetic energy from the mean flow.

d. Transport

Johns et al. (2003) estimated the monthly transport in the southern half of the Strait of Hormuz (approximately along 26°–26.4°N, 56.08°E) for two layers: the variable surface flow of fresher water in the upper layer (0–45 m) and the steady deep outflow of saltier waters in the lower layer (45–100 m). They have used moored current meter data as a proxy for the transport and calibrated it against the four available shipboard velocity sections, and their calculations involved approximations due to a lack of monthly velocity sections. For comparison, the model-derived monthly mean transports for the upper layer during 2005 are shown in Fig. 18a. Model transport varies from a maximum outflow of 0.12 Sv in September 2005 to an inflow of 0.032 Sv in March, which is in approximate agreement with the observed transports of Johns et al. (2003). The annual mean outflow in

the surface layer is 0.04 Sv, which is slightly lower than the observed estimate of 0.06 Sv during 1997.

The transport variability associated with the episodes of enhanced flow is depicted in Figs. 18b and 18c. The estimated transports south and north of 26.4°N along 56.08°E shows a separation between the outflow and inflow. The passage of cyclonic eddies strongly dominates the transport. An abrupt increase in the outflow transport during the passage of eddies accompanies a compensating returning flow in the north. For example, the transport rapidly increases from near zero to 0.3 Sv between mid-March and early April. During nonevent periods, northwesterly winds tend to increase the outflow on the southern part of the strait. To conserve mass, there has to be a compensating returning flow through the northern part of the strait. The converse is true for the southeasterly winds. A comparison of this transport with that obtained from the experiment with no wind stress forcing indicates that the outflow transport is significantly affected by the wind-forced circulation, predominantly during the spring and early summer. The outflow transport between July and December (~0.2 Sv) in both cases is nearly constant. During this period the geostrophy chiefly determines the outflow transport.

4. Summary

Observations in the Strait of Hormuz (26.26°N, 56.08°E) during 1997–98 showed substantial velocity fluctuations, accompanied by episodic changes in the salinity outflow events with amplitudes varying between 1 and 2 psu on time scales of several days to a few weeks (Johns et al. 2003). A high-resolution Hybrid Coordinate Ocean Model (HYCOM) has been successfully applied to simulate the salinity outflow events in the Strait of Hormuz and to validate the results by observational evidence. Model results are in close agreement with the observations. The predominant feature of circulation in the Strait of Hormuz is the establishment of a cyclonic recirculation cell in April that persists until October. The exchange through the strait consists of a highly variable flow in the upper 50 m with frequent reversals and a relatively steady deep outflow below 50 m. The surface layer flow exhibits strong temporal variability predominantly on synoptic time scales (ranges from days to weeks) and causes considerable variability in the salinity outflow. This results in the formation of strong pulses of salinity events, which are characterized by a rapid increase in salinity followed by an abrupt decline. The period of these events is about 15–30 days and their amplitudes often reach up to 2 psu, especially during winter and spring.

The spatial and temporal evolutionary patterns of these high-salinity events clearly indicate that they are

collected at varying phases of the passage of cyclonic mesoscale eddies. These cyclonic eddies originate as an outflow and their formation region can be traced upstream to 26°N, 55.5°E. Thus, the salinity fluctuations in the strait (26.26°N, 56.08°E) observed by Johns et al. (2003) appeared to have an origin farther upstream. Although generation and propagation of the mesoscale eddies are evident throughout the year, they are more pronounced during the spring and summer months. It is during this time that the low-salinity inflow is stronger and results in a marked variation in the stratification and strength of the horizontal salinity (density) gradient across the strait.

The barotropic instability of the exchange circulation through the Strait of Hormuz appears to be the primary process that acts to generate mesoscale cyclonic eddies. The fact that these eddies originate farther upstream (26°N, 55.5°E) from the strait suggests that they are not likely generated from the sheared zonal flows. Abrupt changes in the circulation (in both magnitude and direction) can trigger eddies through local instabilities. Temporal changes in flows can be induced by changes in wind stress forcing or the lateral density gradient or a combination of the two. On shorter time scales, the fluctuations in exchange circulation in the strait are mostly wind driven and barotropic (flow consists of variable Ekman flow, depth-independent geostrophic flow, and possibly other ageostrophic components). Analysis of the wind vectors over the Persian Gulf shows strong shorter-scale temporal variabilities in both magnitude and direction similar to the episodic variations in the outflow through the Strait of Hormuz. Furthermore, the lack of episodic variations in the salinity outflow in a model experiment with no wind stress forcing demonstrates that it is the changes in wind stress forcing that are causing the generation of the variability in the salinity outflow. In the absence of a variable Ekman flow component, the relatively steady exchange circulation through the Strait of Hormuz, driven by the geostrophy alone, is not capable of producing eddies through barotropic instability. Inspection of the energy transfer terms points toward the importance of the transfer of energy from mean to eddy (barotropic instability) due to high-frequency wind forcing as the primary mechanism of eddy generation.

The sequence of events leading to the episodic variations in the salinity outflow can be summarized as follows. The fluctuations in the wind stress forcing drive a variable flow through the Strait of Hormuz. This variable exchange circulation produces local instabilities and generates cyclonic eddies. These cyclones form rather abruptly in the vicinity of 26°N, 55.5°E, where a large portion of the inflow is constrained and guided by
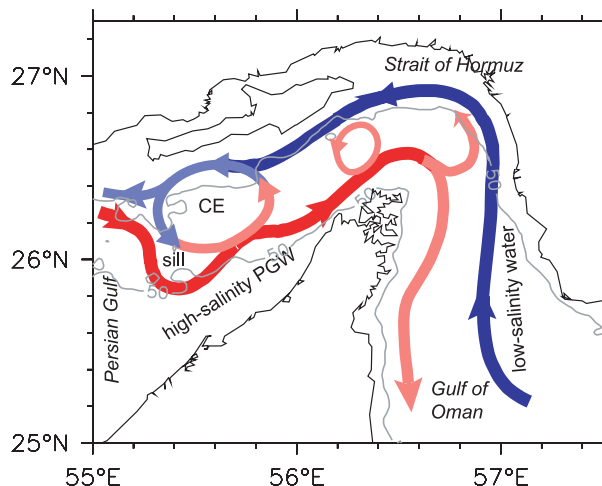

FIG. 19. Schematics diagram of the exchange circulation in the Strait of Hormuz. Shown in gray are 50-m isobaths. Cold-colored (blue to light blue) arrows indicate the inflow of low-salinity water from the Gulf of Oman along the northern part of the strait and warm-colored (red to light red) arrows show the outflow of high-salinity PGW in the south. At 26°N, 55.4°E, a portion of the inflow turns seaward, where the flow is constrained by the sill and narrow channel widths. This seaward current provides an initial location for cyclonic eddies (CEs) to develop and evolve. The variable exchange circulation driven by fluctuations in wind stress forcing generate CEs through BTIs. Coincident with this rapid change in the circulation, the sharp salinity front separating the high-salinity outflow and low-salinity inflow also contributes to the progress of the instabilities. After the formation in the vicinity of ~26°N, 55.4°E, these CEs move downstream at an average speed of 4.1 cm s⁻¹, transporting PGW. As these eddies move downstream, the entrainment and mixing along their path weaken the eddy characteristics.

the highly variable bathymetry features (sill and narrow channels). This constrained flow, in concert with a strong lateral density gradient at this location, forces an offshore current (southward current) that joins the outflow. This offshore current provides an ideal location for cyclonic eddies to develop and evolve. The cyclones have a diameter of about 63 km and they move downstream (northeast) at a translation speed of ~4.1 cm s⁻¹ and are instrumental in transporting heat and salt across the Strait of Hormuz into the Gulf of Oman. The high-salinity PGW in the core of these eddies is eroded by lateral mixing as the eddies propagate downstream. The eddy amplitude decreases farther downstream and eventually loses its characteristics. A schematic diagram showing these processes is depicted in Fig. 19.

We have examined only a few aspects of the outflow variability observed in the Strait of Hormuz. What we have shown here is the remarkable outflow variability dominated by the continuous formation of cyclonic eddies. A comparison of an earlier study (Johns et al. 2003) in this region reveals considerable variability in

the outflow on interannual time scales. In particular, the number and timing of high-salinity events are subject to strong variability that can be associated with the changes in high-frequency wind stress forcings. Future observational programs are necessary to observe the formation and propagation of the cyclonic eddies, and to test the realism of the simulated mode of variability. Further modeling studies are needed to investigate the topographic influence on the formation of eddies, especially the sill depth. Although the simulated salinity qualitatively agrees with the observations, additional experiments with no salinity relaxation would be required to test the model's ability to produce water mass formation. Nevertheless, such attempts would not affect the major conclusions drawn in this study.

REFERENCES

Banse, K., 1997: Irregular flow of Persian (Arabian) Gulf water to the Arabian Sea. *J. Mar. Res.,* **55,** 1049–1067.

Bleck, R., G. R. Halliwell, A. J. Wallcraft, S. Carroll, K. Kelly, and K. Rushing, Hybrid Coordinate Ocean Model (HYCOM) user's manual: Details of the numerical code. HYCOM Consortium, 211 pp. [Available online at http://hycom.rsmas.miami.edu.]

Böning, W. C., and R. G. Budich, 1992: Eddy dynamics in a primitive equation model: Sensitivity to horizontal resolution and friction. *J. Phys. Oceanogr.,* **22,** 361–381.

Bower, A. S., H. D. Hunt, and J. F. Price, 2000: Character and dynamics of the Red Sea and Persian Gulf outflows. *J. Geophys. Res.,* **105** (C3), 6387–6414.

Brewer, P. G., A. P. Fleer, S. Kadar, D. K. Shafer, and C. L. Smith, 1978: Chemical oceanographic data from the Persian Gulf and Gulf of Oman. WHOI Rep. 78-37, Woods Hole Oceanographic Institution, Woods Hole, MA, 105 pp.

Canuto, V. M., A. Howard, Y. Cheng, and M. S. Dubovikov, 2001: Ocean turbulence. Part I: One-point closure model—Momentum and heat vertical diffusivities. *J. Phys. Oceanogr.,* **31,** 1413–1426.

——, ——, ——, and ——, 2002: Ocean turbulence. Part II: Vertical diffusivities of momentum, heat, salt, mass, and passive scalars. *J. Phys. Oceanogr.,* **32,** 240–264.

——, ——, P. J. Hogan, Y. Cheng, M. S. Dubovikov, and L. M. Montenegro, 2004: Modeling ocean deep convection. *Ocean Modell.,* **7,** 75–95.

Chao, S.-Y., T. W. Kao, and K. R. Al-Hajri, 1992: A numerical investigation of circulation in the Arabian Gulf. *J. Geophys. Res.,* **97,** 11 219–11 236.

Horton, C., M. Clifford, J. Schmitz, and B. Hester, 1994: SWAFS: Shallow water analysis and forecast system: Overview and status report. Naval Oceanographic Office, Stennis Space Center, MS, 53 pp.

Hunter, J. R., 1986: The physical oceanography of the Arabian Gulf: A review and theoretical interpretation of previous observations. *Marine Environment and Pollution: Proc. First Arabian Gulf Conference on Environment and Pollution,* Kuwait City, Kuwait, Kuwait University, 1–23.

Johns, W. E., F. Yao, D. B. Olson, S. A. Josey, J. P. Grist, and D. A. Smeed, 2003: Observations of seasonal exchange through the Straits of Hormuz and the inferred freshwater budgets of the Persian Gulf. *J. Geophys. Res.,* **108,** 3391, doi:10.1029/2003JC001881.

Kara, A. B., P. A. Rochford, and H. E. Hurlburt, 2002: Air–sea flux estimates and the 1997–1998 ENSO event. *Bound.-Layer Meteor.,* **103,** 439–458.

——, A. J. Wallcraft, and H. E. Hurlburt, 2007: A correction for land contamination of atmospheric variables near land–sea boundaries. *J. Phys. Oceanogr.,* **37,** 803–818.

Meshal, A. H., and H. M. Hassan, 1986: Evaporation from the coastal waters of the central part of the Gulf. *Arab. Gulf J. Sci. Res.,* **4,** 649–655.

Pous, S. P., X. Carton, and P. Lazure, 2004a: Hydrology and circulation in the Strait of Hormuz and the Gulf of Oman—Results from the GOGP99 experiment: 1. Strait of Hormuz. *J. Geophys. Res.,* **109,** C12037, doi:10.1029/2003JC002145.

——, ——, and ——, 2004b: Hydrology and circulation in the Strait of Hormuz and the Gulf of Oman—Results from the GOGP99 experiment: 2. Gulf of Oman. *J. Geophys. Res.,* **109,** C12038, doi:10.1029/2003JC002146.

Privett, D. W., 1959: Monthly charts of evaporation from the north Indian Ocean, including the Red Sea and the Persian Gulf. *Quart. J. Roy. Meteor. Soc.,* **85,** 424–428.

Reynolds, R. M., 1993: Physical oceanography of the Gulf, Strait of Hormuz and the Gulf of Oman—Results from the Mt Mitchell expedition. *Mar. Pollut. Bull.,* **27,** 35–59.

Swift, S. A., and A. S. Bower, 2003: Formation and circulation of dense water in the Persian/Arabian Gulf. *J. Geophys. Res.,* **108,** 3004, doi:10.1029/2002JC001360.